The Plant Cell, Vol. 10, 267–282, February 1998

AtMRP2, an Arabidopsis ATP Binding Cassette Transporter Able to Transport Glutathione *S*-Conjugates and Chlorophyll Catabolites: Functional Comparisons with AtMRP1

Yu-Ping Lu,[a,1] Ze-Sheng Li,[a,1] Yolanda M. Drozdowicz,[a] Stefan Hörtensteiner,[b] Enrico Martinoia,[c] and Philip A. Rea[a,2]

[a]Plant Science Institute, Department of Biology, University of Pennsylvania, Philadelphia, Pennsylvania 19104-6018
[b]Department of Plant Biology, University of Zurich, CH-8008 Zurich, Switzerland
[c]Institut de Botanique, Université de Neuchâtel, 2007 Neuchâtel, Switzerland

Three ATP binding cassette (ABC) transporter–like activities directed toward large amphipathic organic anions have recently been identified on the vacuolar membrane of plant cells. These are the Mg-ATP–energized, vanadate-inhibitable vacuolar accumulation of glutathione *S*-conjugates (GS conjugates), chlorophyll catabolites, and bile acids, respectively. Although each of these activities previously had been assigned to distinct pumps in native plant membranes, we describe here the molecular cloning, physical mapping, and heterologous expression of a gene, *AtMRP2*, from *Arabidopsis thaliana* that encodes a multispecific ABC transporter competent in the transport of both GS conjugates and chlorophyll catabolites. Unlike its isoform, AtMRP1, which transports the model *Brassica napus* chlorophyll catabolite transporter substrate *Bn*-NCC-1 at low efficiency, heterologously expressed AtMRP2 has the facility for simultaneous high-efficiency parallel transport of GS conjugates and *Bn*-NCC-1. The properties of AtMRP2 therefore establish a basis for the manipulation of two previously identified plant ABC transporter activities and provide an explanation for how the comparable transporter in native plant membranes would be systematically mistaken for two distinct transporters. These findings are discussed with respect to the functional organization of AtMRP2, the inability of AtMRP2 and AtMRP1 to transport the model bile acid transporter substrate taurocholate (despite the pronounced sensitivity of both to direct inhibition by this agent), the differential patterns of expression of their genes in the intact plant, and the high capacity of AtMRP2 for the transport of glutathionated herbicides and anthocyanins.

INTRODUCTION

Recent studies have identified a new type of organic solute transporter activity in plants. These transporters, contrary to the prevailing chemosmotic model for energy-dependent transport in plants, are directly energized by Mg-ATP rather than by a transmembrane H^+-electrochemical potential difference established by the action of H^+-ATPases and H^+-pyrophosphatases. Three of the most thoroughly characterized of these activities are those implicated in the transport of large amphipathic organic anions into the vacuole. The first, a glutathione *S*-conjugate (GS conjugate) pump, transports glutathionated compounds and oxidized glutathione (GSSG) (Figure 1) (Martinoia et al., 1993; Li et al., 1995a, 1995b, 1997a; Blake-Kalff and Coleman, 1996) and is considered to participate in the vacuolar sequestration of glutathione (GSH)-conjugable compounds. The second, the in vivo function of which is not known, is competent in the transport of bile acids, such as taurocholate, a taurinylated derivative of cholate (Figure 1) (Hörtensteiner et al., 1993). The third, which may play a role in the excretion storage of linear tetrapyrroles derived from the catabolism of chlorophyll during leaf senescence, transports *Bn*-NCC-1, a malonyl ester of the predominant nonfluorescent chlorophyll catabolite from *Brassica napus* (Figure 1), at high capacity (Hinder et al., 1996). All three transport functions are directly energized by nucleoside triphosphates (primarily the magnesium salt of ATP, Mg-ATP), insensitive to agents that dissipate transmembrane H^+ gradients, and strongly inhibited by micromolar concentrations of the phosphoryl transition state analog vanadate.

Pivotal for mechanistic investigations of these and related transport functions in plants is the recent isolation of a gene (*AtMRP1*) from *Arabidopsis thaliana* that encodes an ATP binding cassette (ABC) transporter capable of transporting GS conjugates (Lu et al., 1997). AtMRP1 is both a structural and functional homolog of the human multidrug resistance–associated protein (*HmMRP1*) gene product (Cole et al., 1992), which has been identified on the basis of its ability to confer GS conjugate pump activity on transfected cells (Leier et al.,

[1]These authors contributed equally to this work.
[2]To whom correspondence should be addressed. E-mail parea@sas.upenn.edu; fax 215-898-8780.

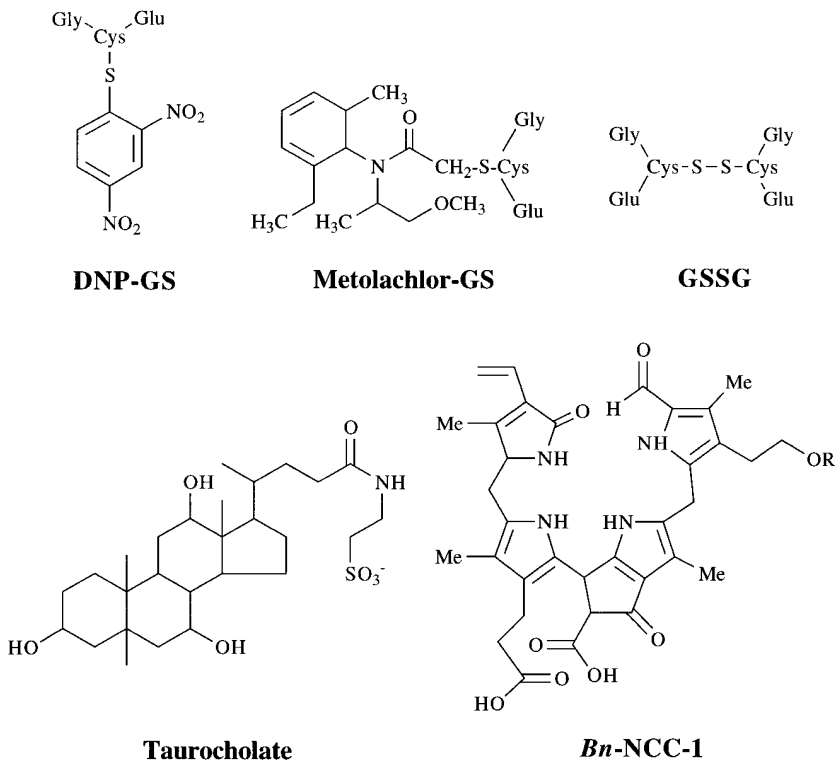

Figure 1. Structures of the Compounds Used in This Study.

Shown are *S*-(2,4-dinitrophenyl)glutathione (DNP-GS), glutathionated metolachlor (metolachlor-GS), oxidized glutathione (GSSG), taurinylated cholate (taurocholate), and the *B. napus* chlorophyll catabolite *Bn*-NCC-1. R, malonyl group.

1994; Muller et al., 1994), and the *Saccharomyces cerevisiae* (yeast) cadmium factor (*ScYCF1*) gene product (Szczypka et al., 1994), which is a vacuolar GS conjugate pump (Li et al., 1996, 1997a; Tommasini et al., 1996). AtMRP1, HmMRP1, and ScYCF1 possess the same overall domain organizations and catalyze Mg-ATP–energized, vanadate-inhibitable transport of GS conjugates and GSSG.

In addition to their strategic value for manipulating the transport processes underlying GSH-dependent xenobiotic and endogenous toxin metabolism in plants, the molecular isolation and functional definition of *AtMRP1* are significant at two levels. First, they represent the combined molecular and biochemical characterization of an ABC transporter from a plant source. Despite their ubiquity and involvement in the transport of a broad range of substances in representative organisms from most of the major taxa (Higgins, 1992) and the isolation of multidrug resistance protein–like ABC transporter genes from Arabidopsis (Dudler and Hertig, 1992), potato (Wang et al., 1996), and barley (Davies et al., 1997), no transport function had been assigned directly to a plant ABC transporter. Second, they might provide a rational basis for understanding a number of other ABC transporter–like activities in plants.

Accumulating evidence from studies of the MRP subclass members from non-plant sources reveals that the group of transporters formerly referred to as GS-*X* pumps because of their affinity toward GS conjugates, GSSG, and cysteinyl leukotrienes does not transport GS conjugates exclusively (Ishikawa et al., 1997). Although the initial molecular identification of a GS-*X* pump arose from the demonstration that overexpression of *HmMRP1* confers increased Mg-ATP–energized GS conjugate transport (Leier et al., 1994; Muller et al., 1994), subsequent investigations of HmMRP1 itself, the canalicular multispecific organic anion transporter (cMOAT; Paulusma et al., 1996), and ScYCF1 have shown the GS-*X* pump concept to be too restrictive (Ishikawa et al., 1997). Each of these representatives from the MRP subclass can transport a broad range of compounds in addition to GS conjugates and GSSG. HmMRP1 is able to transport glucuronidated and sulfated compounds, such as glucuronosyl estradiol and sulfatolithocholyltaurine (Jedlitschky et al., 1996); cMOAT, a liver-specific isoform of MRP1, is able to transport bile acids (Paulusma et al., 1996), bilirubin glucuronide, cysteinyl leukotrienes (Huber et al., 1987; Ishikawa et al., 1990), and unconjugated organic acids, such as bromosulfphthalein and indocyanine green (Sathirakul et al., 1993);

ScYCF1 is able to transport heavy metals after they have been complexed with GSH (Li et al., 1997b).

Against this background and on the basis of the remarkable structural resemblance of AtMRP1 to these other MRP subclass pumps (Lu et al., 1997), several interrelated questions must be addressed. Does AtMRP1 transport GS conjugates exclusively or can it also transport other bulky anions? Is *AtMRP1* a member of a multigene family in Arabidopsis, as is the case for MRP subclass genes from other organisms? If so, do the other family members possess transport capabilities distinct from or overlapping with those of AtMRP1? Given that all three of the plant ABC transporter–like transport functions described above involve Mg-ATP–energized, vanadate-inhibitable transport of bulky amphipathic organic anions, is AtMRP1 and/or related membrane proteins able to satisfy one or more of these transport functions?

Although it has been argued that vacuolar uptake of GS conjugates, bile salts, and chlorophyll catabolites is catalyzed by distinct transporters, the evidence in support of this is indirect and somewhat conflicting. Hinder et al. (1996) suggest that the transport function responsible for Mg-ATP–energized uptake of the chlorophyll catabolite *Bn*-NCC-1 into isolated vacuoles from barley is different from those responsible for the uptake of GS conjugates and taurocholate because neither of the latter two classes of compound compete with *Bn*-NCC-1 for uptake. Nevertheless, the same authors in the same study find that another GS conjugate, decyl-GS, does compete with *Bn*-NCC-1 for uptake. Similarly, although Hörtensteiner et al. (1993) suggest that GS conjugate and taurocholate transport are mediated by different pumps because the model GS conjugate *S*-(2,4-dinitrophenyl)glutathione (DNP-GS) and the glutathionated chloroacetanilide herbicide metolachlor-GS do not inhibit taurocholate uptake into barley vacuoles, Blake-Kalff and Coleman (1996) in a reciprocal experiment using the same preparation found that uptake of another model GS conjugate, *N*-ethylmaleimide-GS (NEM-GS), is inhibited by taurocholate. Evidently, interpretative difficulties arise when competition is the principal criterion for deciding whether two or more candidate transport substrates use the same transport pathway and when preparations (plant vacuoles or vacuolar membrane vesicles), likely containing several transporters with overlapping substrate specificities, are the sole experimental material available.

In this article, we describe the isolation of a second gene, *AtMRP2*, from Arabidopsis that belongs to the same subclass of ABC transporter genes as *AtMRP1*, whose heterologous expression in yeast also confers Mg-ATP–energized GS conjugate transport. Because plasmid-borne *AtMRP2* and *AtMRP1* are functionally expressed in mutant yeast strains otherwise deficient in vacuolar GS conjugate transport, the availability of both genes provided a unique opportunity for comparing their individual transport capabilities and substrate specificities without interference from related transport functions. From kinetic analyses of each transporter, we demonstrate that heterologous AtMRP2 not only has a GS conjugate transport activity severalfold greater than that of AtMRP1 but is also capable of high-affinity, high-capacity transport of *Bn*-NCC-1. This is a property not shared by AtMRP1. The unusual modes of interaction of AtMRP2 with GS conjugates and *Bn*-NCC-1 and of both AtMRP2 and AtMRP1 with taurocholate confirm the limitations of inferences drawn from simple kinetic measurements using native plant membranes and demonstrate AtMRP2's facility for the parallel transport of GS conjugates and chlorophyll catabolites. We conclude that AtMRP2 is a multispecific ABC transporter active in the semiautonomous transport of both glutathionated and nonglutathionated compounds.

RESULTS

Isolation of *AtMRP2*

On the basis of the functional resemblance of plant vacuolar GS conjugate transport to that mediated by ScYCF1 and HmMRP1 and the 44.6% sequence identity (63.9% similarity) between ScYCF1 and HmMRP1, degenerate oligonucleotide primers corresponding to the second ATP binding cassette of ScYCF1 and HmMRP1—two of the most ScYCF1- and HmMRP1-specific sequences common to both—were used to initiate the isolation of plant genes likely involved in GS conjugate transport by polymerase chain reaction (PCR) amplification of Arabidopsis genomic DNA. This procedure yielded a 0.6-kb Arabidopsis amplification product that hybridized with the equivalent PCR products of *ScYCF1* and *HmMRP1.* Sequence analysis demonstrated that the 0.6-kb product comprised a 76-bp intron and 510-bp exon, the latter of which shared 60.6 and 66.5% amino acid sequence identity with the corresponding regions of ScYCF1 and HmMRP1 and complete nucleotide sequence identity with the 5′ segment of a 1.6-kb Arabidopsis expressed sequence tag (EST), ATTS1246 (Hofte et al., 1993). Because their deduced amino acid sequences are as similar to ScYCF1 and HmMRP1 as ScYCF1 and HmMRP1 are to each other, the Arabidopsis PCR product and EST were used as probes for the isolation of full-length clones.

Full-length clones were isolated in three stages. A cDNA library was screened with a mixed probe consisting of the 0.6-kb PCR product and EST to isolate a partial (3.5-kb) clone exhibiting 42.5 and 43.5% amino acid identity to ScYCF1 and HmMRP1, respectively; two bacterial artificial chromosome (BAC) libraries were screened with a probe corresponding to 0.5 kb of the most 5′ portion of the 3.5-kb cDNA to isolate eight clones, of which two (U1L22 and U12A2) encompassed the entire cDNA sequence; total RNA from Arabidopsis was subjected to reverse transcriptase (RT)–PCR to recover the missing 5′ cDNA sequence for reconstruction of the complete open reading frame. After verifying that the final cDNA was derived from Arabidopsis rather than from a non-plant contaminant of the cDNA library by

RNA gel blot analysis (below), the complete sequences of the cDNA and appropriate restriction fragments of genomic clones U1L22 and U12A2 were determined.

Sequence and Physical Map Position of *AtMRP2*

The genomic sequence of *AtMRP2* contained a total of 28 introns and mapped to a position between the Ve016 and Ve018 loci on chromosome 2 (Figure 2). The single open reading frame of the cDNA corresponding to this gene encoded a 1623–amino acid residue (181 kD) polypeptide exhibiting 87% overall sequence identity (94% similarity) to AtMRP1 and 36, 38, and 40% sequence identity (56, 59, and 63% similarity) to ScYCF1, HmMRP1, and rat cMOAT (RtCMOAT), respectively. As revealed by application of the program Phylogenetic Analysis Using Parsimony (PAUP) to the protein sequences of a broad range of representative ABC transporters, AtMRP2 belonged only to the MRP subclass—a subclass adjacent to the cystic fibrosis transmem-

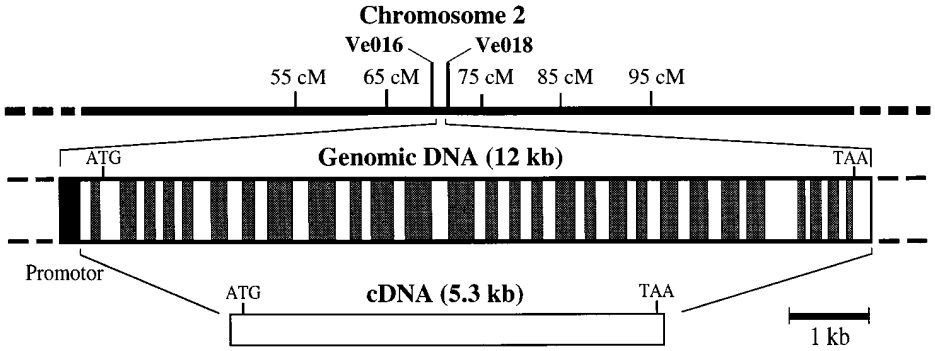


```
   1 MGFEFIEWYCKPVPNGVWTKTVANAFGAYTPCATDSFVLGISQLVLLVLCLYRIWLALKDHKVE
  65 RFCLRSRLYNYFLALLAAYATAEPLFRLIMGISVLDFDGPGLPPFEAFGLGVKAFAWGAVMVMI
 129 LMETKIYIRELRWYVRFAVIYALVGDMVLLNLVLSVKEYYSSYVLYLYTSEVGAQVLFGILLFM
 193 HLPNLDTYPGYMPVRSETVDDYEYEEISDGQQICPEKHPNIFDKIFFSWMNPLMTLGSKRPLTE
 257 KDVWYLDTWDQTETLFTSFQHSWDKELQKPQPWLLRALNNSLGGRFWWGGFWKIGNDCSQFVGP
 321 LLLNQLLKSMQEDAPAWMGYIYAFSIFGGVVFGVLCEAQYFQNVMRVGYRLRSALIAAVFRKSL
 385 RLTNEGRRKFQTGKITNLMTTDAESLQQICQSLHTMWSAPFRIIIALILLYQQLGVASLIGALL
 449 LVLMFPLQTVIISKMQKLTKEGLQRTDKRIGLMNEVLAAMDTVKCYAWENSFQSKVQTVRDDEL
 513 SWFRKSQLLGALNMFILNSIPVLVTIVSFGVFTLLGGDLTPARAFTSLSLFAVLRFPLFMLPNI
 577 ITQVVNANVSLNRLEEVLATEERILLPNPPIEPGEPAISIRNGYFSWDSKGDRPTLSNINLDVP
 641 LGSLVAVVGSTGEGKTSLISAILGELPATSDAIVTLRGSVAYVPQVSWIFNATVRDNILFGSPF
 705 DREKYERAIDVTSLKHDLELLPGGDLTEIGERGVNISGGQKQRVSMARAVYSNSDVYIFDDPLS
 769 ALDAHVGQQVFEKCIKRELGQKTRVLVTNQLHFLSQVDRIVLVHEGTVKEEGTYEELSSNGPLF
 833 QRLMENAGKVEEYSEENGEAEADQTAEQPVANGNTNGLQMDGSDDKKSKEGNKKGGKSVLIKQE
 897 ERETGVVSWRVLKRYQDALGGAWVVMMLLLCYVLTEVFRVTSSTWLSEWTDAGTPKSHGPLFYN
 961 LIYALLSFGQVLVTLTNSYWLIMSSLYAAKKLHDNMLHSILRAPMSFFHTNPLGRIINRFAKDL
1025 GDIDRTVAVFVNMFMGQVSQLLSTVVLIGIVSTLSLWAIMPLLVLFYGAYLYYQNTAREVKRMD
1089 SISRSPVYAQFGEALNGLSTIRAYKAYDRMADINGRSMDNNIRFTLVNMGANRWLGIRLETLGG
1153 LMIWLTASFAVMQNGRAENQQAFASTMGLLLSYALNITSLLTGVLRLASLAENSLNAVERVGNY
1217 IEIPPEAPPVIENNRPPPGWPSSGSIKFEDVVLRYRPQLPPVLHGVSFFIHPTDKVGIVGRTGA
1281 GKSSLLNALFRIVEVEEGRILIDDCDVGKFGLMDLRKVLGIIPQSPVLFSGTVRFNLDPFGEHN
1345 DADLWESLERAHLKDTIRRNPLGLDAEVSEAGENFSVGQRQLLSLSRALLRRSKILVLDEATAA
1409 VDVRTDALIQKTIREEFKSCTMLIIAHRLNTIIDCDKILVLDSGRVQEFSSPENLLSNEGSSFS
1473 KMVQSTGAANAEYLRSLVLDNKRAKDDSHHLQGQRKWLASSRWAAAAQFALAASLTSSHNDLQS
1537 LEIEDDSSILKRTNDAVVTLRSVLEGKHDKEIAESLEEHNISREGWLSSLYRMVEGLAVMSRLA
1601 RNRMQQPDYNFEGNTFDWDNVEM
```

Figure 2. Genomic Organization of *AtMRP2*, Nucleotide Sequence of *AtMRP2* cDNA, and Deduced Amino Acid Sequence of AtMRP2.

The relative positions and sizes of the introns and exons of the genomic clone, determined by comparison with the cDNA sequence, are indicated by shaded and open rectangles, respectively. The Walker A and B motifs (sequences GSTGEG and GRTGAG, and VYIFD and ILVLD, respectively) and the ABC signature motifs (sequences SGGQKQRVSMA and FSVGQRQLLSLS) of the deduced amino acid sequence of AtMRP2 are indicated by white text on a black background. The N-terminal extension and CFTR-like truncated regulatory domain (R) are indicated by underlined roman letters and italic boldface letters, respectively. Putative transmembrane spans were identified using the TopPred II program (M.G. Claros and G. von Heijne, Karolinska Institute, Stockholm, Sweden) and are indicated by roman boldface letters. The positions and directions of the two PCR primers used to amplify Arabidopsis genomic DNA during the initial stages of cloning *AtMRP2* are indicated by arrows. cM, centimorgan.

brane conductance regulator protein (CFTR) cluster. Although PAUP analysis showed three other ABC transporters for which GS-*X* activity has yet to be examined—the rabbit epithelial basolateral conductance regulator (RbEBCR), Leishmania P-glycoprotein–related molecule (LePGP1), and yeast oligomycin resistance protein (ScYOR1)—to fall into the same subclass as AtMRP2, AtMRP1, ScYCF1, HmMRP1, and RtCMOAT (Figure 3A), this cluster was remote from those incorporating the multidrug resistance proteins, MHC class II–linked peptide transporters, *Schizosaccharomyces pombe* heavy metal tolerance protein (SpHMT1), and *S. cerevisiae* mating factor export protein (ScSTE6) (data not shown).

AtMRP2, like AtMRP1 and other members of the MRP subclass (Lu et al., 1997), possesses two nucleotide binding folds (NBF1 and NBF2). Each contains the Walker A and B motifs and C motif characteristic of ABC transporters (Higgins, 1992) (Figure 2), 12 putative transmembrane spans (Figure 2), and two subclass-specific structures that include a putative "regulatory" (R) domain contiguous with NBF1, rich in charged amino acids (Figure 2), and common to the MRP and CFTR subclasses but truncated in the former subclass (117 to 161 versus 256 amino acid residues), and a 192– to 223–amino acid residue N-terminal extension containing five hydrophilicity minima, which are absent from the CFTR subclass but present in all MRP subclass members (Figures 2 and 3B).

Expression of *AtMRP2* and *AtMRP1* in Arabidopsis

AtMRP2-specific transcript was detected in all of the Arabidopsis tissues examined, confirming that the cDNA was indeed derived from this organism and not from a contaminant of the cDNA library; however, its steady state levels were considerably lower than those of *AtMRP1.* Gel blot analyses of total RNA extracted from roots, leaves, stems, and flowers of 5-week-old plants probed with a gene-specific riboprobe corresponding to the 3′ untranslated region of *AtMRP2* yielded a single 5.3-kb hybridizing band whose intensity was low and similar in all of the tissues examined (Figure 4). By contrast, the same blots probed with an *AtMRP1*-specific 3′ riboprobe yielded an intense 5.3-kb hybridizing band in the RNA samples from leaves and stems, a band of intermediate intensity in the samples from flowers, and a band of low intensity in those from roots (Figure 4). *AtMRP1* transcript levels in roots were approximately sixfold lower than in flowers and 10- to 16-fold lower than in leaves and stems, respectively, and five- to 36-fold greater than those of *AtMRP2.*

AtMRP2-Mediated DNP-GS Transport

To determine whether the structural resemblance of AtMRP2 to AtMRP1 and other members of the MRP subclass had a functional basis, we examined the capacity of heterologously expressed AtMRP2 for Mg-ATP–energized, uncoupler-insensitive GS conjugate transport. For this purpose, *S. cerevisiae ycf1Δ* strain DTY168, from which 95% of the coding sequence of the *YCF1* gene had been deleted (Szczypka et al., 1994) and high-affinity, Mg-ATP–dependent, uncoupler-insensitive vacuolar GS conjugate transport is abolished (Li et al., 1996, 1997b; Tommasini et al., 1997), was transformed with empty expression vector (pYES3) or the vector containing the entire open reading frame of *AtMRP2* (pYES3-AtMRP2) under the control of the constitutive yeast phosphoglycerate kinase gene (*PGK*) promoter. After growth on selective media, vacuolar membrane–enriched vesicles (Kim et al., 1995) were prepared from these and untransformed DTY168 cells and assayed for transport of the model GS conjugate DNP-GS.

The vector alone had negligible effect on uncoupler-insensitive DNP-GS uptake, implying that the cDNA insert of pYES3-AtMRP2 was responsible for the increases in transport measured (Figure 5A). When assayed at an initial ^{3}H–DNP-GS concentration of 61.3 μM, the rates of Mg-ATP–dependent uncoupler-insensitive uptake by vacuolar membrane–enriched vesicles purified from untransformed DTY168 cells (DTY168 cells) and pYES3-transformed DTY168 cells (DTY168/pYES3 cells) were indistinguishable and approximately fourfold lower than for the equivalent membrane fraction from pYES3-AtMRP2–transformed DTY168 cells (pYES3-AtMRP2/DTY168 cells) (Figure 5A). Because protonophores (carbonyl *p*-trifluoromethoxyphenylhydrazone [FCCP] and gramicidin D) inhibited total Mg-ATP–dependent uptake by $<$33% and the V-ATPase inhibitor, bafilomycin A_1, did not augment the effects of protonophores (Figure 5B), the increases in Mg-ATP–dependent DNP-GS uptake exhibited by DTY168/pYES3-AtMRP2 membranes were largely independent of the transmembrane H^+ electrochemical potential difference otherwise established by the V-ATPase associated with this membrane preparation (Zhen et al., 1997). A specific requirement for hydrolysis of the γ-phosphoryl group of ATP for the energization of AtMRP2-mediated transport was indicated by the inability of the nonhydrolyzable ATP analog adenosine 5′-(β,γ-imino)triphosphate (AMP-PNP) to support uncoupler-insensitive uptake (Figure 5B).

Uncoupler- and V-ATPase inhibitor–insensitive, Mg-ATP–dependent DNP-GS uptake consisted of two components: (1) an AtMRP2-dependent component accounting for $>$75% of total Mg-ATP–dependent uptake by DTY168/pYES3-AtMRP2 membranes and (2) an AtMRP2-independent component, which was present at the same level in DTY168 and DTY168/pYES3 membranes and accounted for $<$25% of total Mg-ATP–dependent uptake by DTY168/pYES3-AtMRP2 membranes. Of these two components, only the AtMRP2-dependent component was inhibited by vanadate. The rate of Mg-ATP–dependent, uncoupler-insensitive ^{3}H–DNP-GS uptake by DTY168/pYES3-AtMRP2 membranes decreased as a single negative exponential function of vanadate concentration to yield an I_{50} (concentration required for 50% inhibition) of 6.4 ± 0.4 μM (Figure 5A), whereas uptake by DTY168/pYES3 (and DTY168) membranes was insensitive to this agent (Figure 5A).

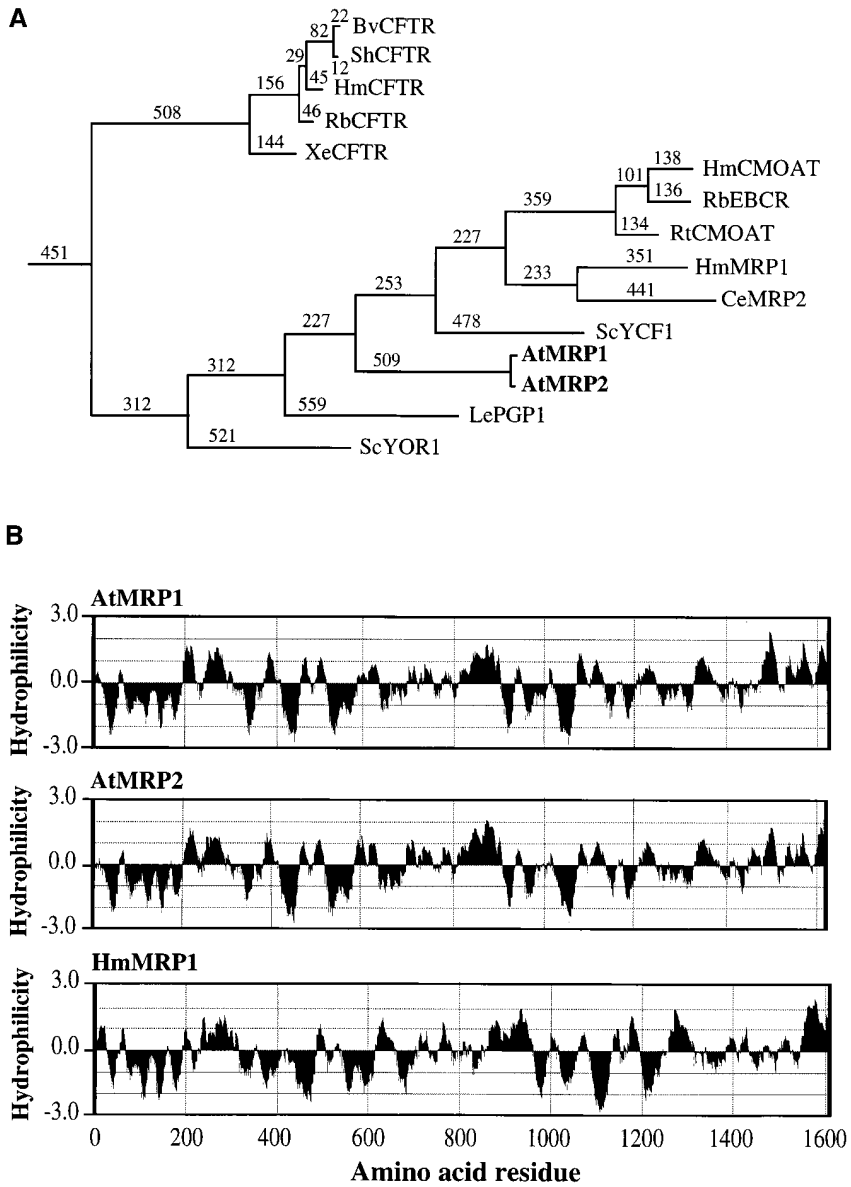

Figure 3. Structural Comparisons of AtMRP2 with Other ABC Transporters.

(A) A portion of a dendrogram constructed using the polypeptide sequences of representative members of the ABC transporter superfamily. Shown is the cluster containing AtMRP2 and AtMRP1. Multiple alignments produced by the PILEUP program (version 8.0; Genetics Computer Group, Madison, WI), with a gap penalty of 3.0 and gap extension penalty of 0.1, were used to generate a dendrogram, using the program Phylogenetic Analysis Using Parsimony (PAUP, version 3.1.1). The protein sequence of AHA10 (GenBank accession number S74033), an Arabidopsis P-type H^+-ATPase, was used as the outgroup for rooting the dendrogram. Numbers above and below lines denote the number of amino acid substitutions between a given polypeptide and its immediate putative progenitor, assuming maximum parsimony. The GenBank/EMBL accession numbers of the ABC transporters used in this comparison are as follows: AF008124 and AF020288, AtMRP1 and AtMRP2, respectively; M76128, U20418, M28668, U40227, and U60209, cystic fibrosis transmembrane conductance regulator protein from cow (BvCFTR), sheep (ShCFTR), human (HmCFTR), rabbit (RbCFTR), and *Xenopus laevis* (XeCFTR), respectively; X96396 and L49379, canalicular multispecific organic anion transporter proteins from human (HmCMOAT) and rat (RtCMOAT), respectively; 249144, rabbit epithelial basolateral chloride conductance regulator (RbEBCR); L05628 and U66261, multidrug resistance–associated proteins from human (HmMRP1) and *Caenorhabditis elegans* (CeMRP2), respectively; L35237, yeast (*S. cerevisiae*) cadmium factor protein (ScYCF1); 1235963, yeast (*S. cerevisiae*) oligomycin resistance protein (ScYOR1); and X17154, P-glycoprotein–related molecule from Leishmania (LePGP1).

(B) Comparison of the hydrophilicity profiles of AtMRP1, AtMRP2, and HmMRP1. Hydrophilicity was computed over a running window of 19 amino acid residues, using the scale of Kyte and Doolittle (1982).

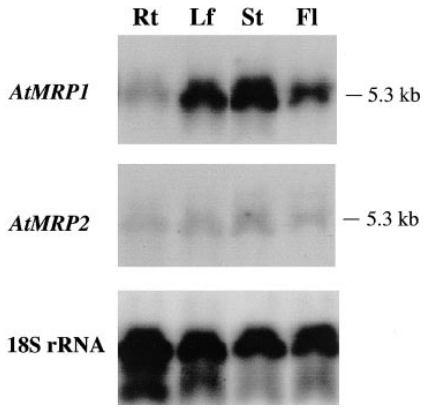

Figure 4. RNA Gel Blot Analyses of the Expression of *AtMRP1* and *AtMRP2* Transcripts in Roots, Leaves, Stems, and Flowers of Arabidopsis.

Total RNA (10 μg per lane) was extracted, separated, blotted, and hybridized with ^{32}P-labeled riboprobes corresponding to the 3′ untranslated regions of *AtMRP1* and *AtMRP2.* The 5.3-kb bands are the only ^{32}P-labeled bands that were detected in the blots probed with *AtMRP1* or *AtMRP2.* Also shown are the results of hybridizing the same blots with a probe directed against the 18S rRNA to verify that similar amounts of RNA had been loaded in each lane. Rt, roots; Lf, leaves; St, stems; Fl, flowers.

Substrate Preferences of AtMRP2 and AtMRP1

Its absence from DTY168 and DTY168/pYES3 membranes and selective inhibition by micromolar concentrations of vanadate meant that AtMRP2-dependent transport could be measured in two ways: either as the difference between the rates of Mg-ATP–dependent, uncoupler-insensitive uptake by DTY168/pYES3-AtMRP2 membranes by comparison with DTY168 or DTY168/pYES3 membranes or as the vanadate-sensitive component of Mg-ATP–dependent, uncoupler-insensitive uptake by DTY168/pYES3-AtMRP2 membranes. Because the results were qualitatively and quantitatively similar whichever method was used, we use the term AtMRP2-dependent transport to refer to uptake measured as the increment consequent on transformation of DTY168 cells with pYES3-AtMRP2 versus pYES3.

Application of this methodology to vacuolar membrane–enriched vesicles purified from pYES3-AtMRP2– versus pYES3-transformed DTY168 cells and expansion of the transport assays to measurements of the concentration dependence of ^{3}H–DNP-GS, ^{3}H-GSSG, ^{14}C–metolachlor-GS, ^{14}C–*Bn*-NCC-1, and ^{3}H-taurocholate uptake demonstrated that the substrate preferences and maximal transport capacities of heterologously expressed AtMRP2 (Figure 6B) and AtMRP1 (Figure 6A) differed markedly. Although uptake of all of the GSH derivatives examined conformed to Michaelis–Menten kinetics, the V_{max} values for AtMRP2-dependent uptake were consistently severalfold greater than those for AtMRP1-dependent uptake (Figure 6 and Table 1). The V_{max} values for AtMRP2-dependent uptake of ^{3}H–DNP-GS, ^{3}H-GSSG, and ^{14}C–metolachlor-GS were 16.3 ± 3.1, 38.1 ± 3.2, and 136.0 ± 28.1 nmol/mg per 10 min, respectively; the corresponding values for AtMRP1 were 8.2 ± 1.6, 6.8 ± 1.1, and 17.5 ± 5.2 nmol/mg per 10 min. With the exception of ^{3}H-GSSG, whose K_m for AtMRP1-dependent uptake (219.2 ± 58.3 μM) was three times greater than that for AtMRP2-dependent uptake (73.0 ± 15.1 μM), the K_m values estimated for AtMRP2 and AtMRP1 were very similar (65.7 ± 29.8 versus 73.8 ± 18.8 μM for DNP-GS; 75.1 ± 31.6 versus 63.6 ± 36.5 μM for metolachlor-GS) (Table 1).

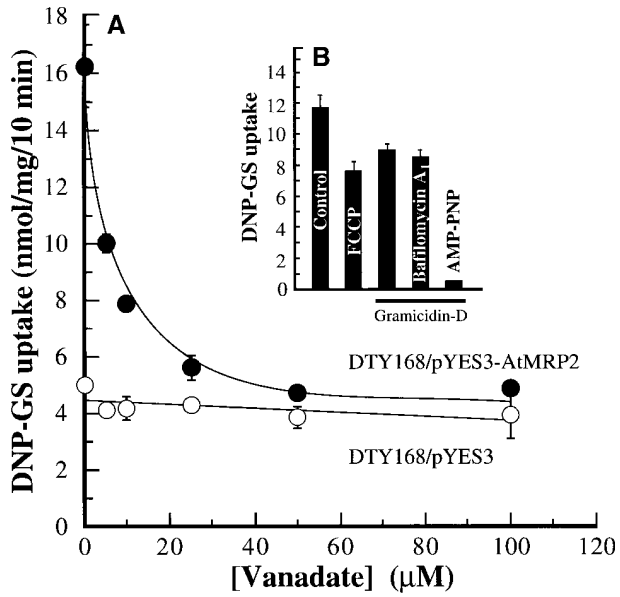

Figure 5. DNP-GS Uptake by Vacuolar Membrane–Enriched Vesicles Purified from *S. cerevisiae ycf1Δ* Strain DTY168 after Transformation with Empty pYES3 Vector (pYES3) or Vector Containing the Coding Sequence of *AtMRP2* (pYES3-AtMRP2).

(A) Sensitivity of Mg-ATP–dependent, uncoupler-insensitive DNP-GS uptake by DTY168/pYES3-AtMRP2 (closed circles) or DTY168/pYES3 membranes (open circles) to inhibition by vanadate.

(B) Effect of protonophores, V-ATPase inhibitor, bafilomycin A_1, and AMP-PNP on Mg-ATP–dependent DNP-GS uptake by vacuolar membrane vesicles purified from DTY168/pYES3-AtMRP2 cells.

In **(A)**, uptake of ^{3}H–DNP-GS was measured in the presence of 5 μM gramicidin D throughout. In **(B)**, gramicidin D was omitted unless otherwise indicated. In **(A)** and **(B)**, ^{3}H–DNP-GS uptake was measured at a concentration of 61.3 μM, and Mg-ATP–dependent uptake was enumerated as the increase in uptake consequent on the provision of 3 mM Mg-ATP. AMP-PNP, bafilomycin A_1, and FCCP were added at concentrations of 3 mM, 0.5 μM, and 5 μM, respectively. The data for inhibition of ^{3}H–DNP-GS uptake by vanadate were fitted to a single negative exponential function by nonlinear least squares analysis (Marquardt, 1963) to yield an I_{50} for inhibition (exclusive of the uninhibitable, AtMRP2-independent component) of 6.4 ± 0.4 μM. Values shown are means ±SE (n = 3).

Single-concentration (50 μM) measurements of uptake of the glutathionated anthocyanin, cyanin-3-glucoside-GS (C3G-GS), demonstrated an approximately sixfold greater capacity of AtMRP2 for transport of this compound (rate = 48.4 ± 2.2 nmol/mg per 10 min) compared with AtMRP1 (rate = 7.9 ± 0.7 nmol/mg per 10 min) (data not shown). In no case was Mg-ATP–dependent, uncoupler-insensitive uptake of the unconjugated precursors of the GS compounds DNP, GSH, metolachlor, and C3G detectable (data not shown).

Neither AtMRP2 nor AtMRP1 catalyzed the uptake of ^{3}H-taurocholate. Transformation of DTY168 cells with either pYES3-AtMRP2 or pYES3-AtMRP1 conferred little or no increase in the capacity of vacuolar membrane–enriched vesicles for ^{3}H-taurocholate uptake over that measured with vesicles prepared from pYES3-transformed cells (Figure 6).

The two- to eightfold greater capacity of AtMRP2 versus AtMRP1 for transport of the compounds examined was not attributable to differences in the levels of transcription of their cDNAs from the *PGK* gene promoter of pYES3. Quantitative RT-PCR of equivalent amounts of total RNA extracted from DTY168/pYES3-AtMRP2 and DTY168/pYES3-AtMRP1 cells yielded similar levels of the 800-bp PCR amplification product predicted from the sequences of the oligonucleotide primers used (Figure 7). Because neither amplification product was generated when PCR was performed without reverse transcription or when total RNA from DTY168/pYES3 cells was used as template (Figure 7), contamination by genomic DNA and/or RT-PCR of transcripts other than those from *AtMRP2* or *AtMRP1*, respectively, was not responsible for the results.

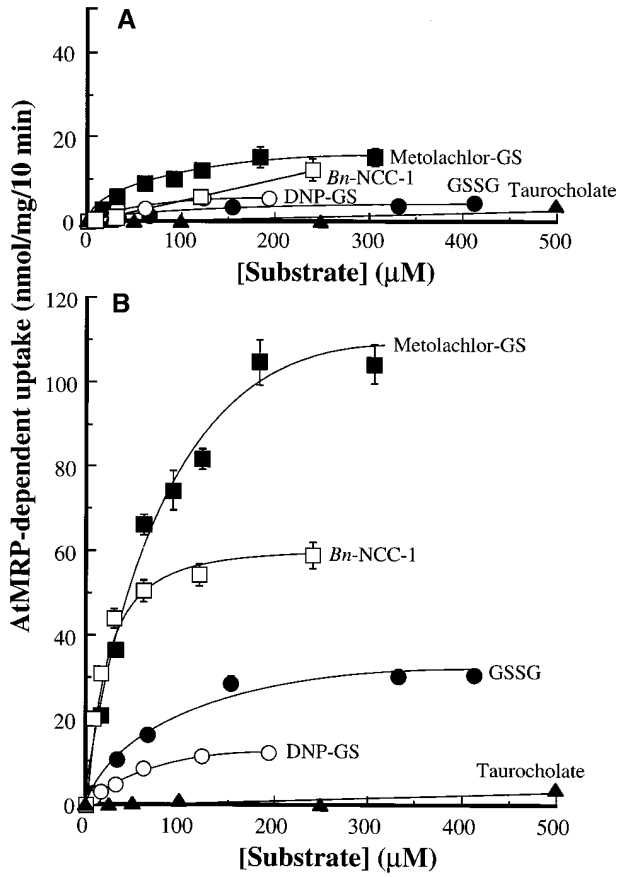

Figure 6. Concentration Dependence of AtMRP1- and AtMRP2-Dependent Uptake of ^{14}C–*Bn*-NCC-1, ^{3}H–DNP-GS, ^{3}H-GSSG, ^{14}C–Metolachlor-GS, and ^{3}H-Taurocholate.

(A) AtMRP1-dependent uptake.

(B) AtMRP2-dependent uptake.

The rates of AtMRP2- and AtMRP1-dependent uptake were calculated by subtracting the radioactivity taken up by vacuolar membrane–enriched vesicles prepared from pYES3-transformed cells from that taken up by the equivalent membrane fraction from pYES3-AtMRP1– or pYES3-AtMRP2–transformed DTY168 cells. All of the data were fitted to a single Michaelis–Menten function by nonlinear least squares analysis, except those for taurocholate uptake and AtMRP1-dependent *Bn*-NCC-1 uptake, which were fitted to a linear function. The kinetic parameters estimated from these experiments are summarized in Table 1. Values shown are means ±SE (n = 3).

Anomalous Interactions between Candidate Transport Substrates

Two critical properties of AtMRP2 were its capacity for the high-affinity simultaneous transport of GS conjugates and *Bn*-NCC-1 and its pronounced sensitivity to inhibition by taurocholate. Simultaneous measurements of ^{14}C–*Bn*-NCC-1 and ^{3}H–DNP-GS uptake by membrane vesicles purified from DTY168/pYES3-AtMRP2 cells revealed comparable accumulation of both compounds with little or no interference of the transport of one by the other (Figure 8). AtMRP2-dependent uptake of ^{14}C–*Bn*-NCC-1 at an extravesicular concentration equivalent to its K_m value (15 μM; Table 1) was nearly three times less sensitive to DNP-GS than would be predicted if this GS conjugate were a competitor. If DNP-GS were a simple competitive inhibitor such that its K_m value (66 μM; Table 1) approximated its K_i value for the inhibition of *Bn*-NCC-1 uptake, 120 μM DNP-GS would be expected to inhibit ^{14}C–*Bn*-NCC-1 uptake by 48%, but this was not found. DNP-GS concentrations >120 μM decreased ^{14}C–*Bn*-NCC-1 uptake by <18% (Figure 8). Reciprocally, the concentration dependence of AtMRP2-mediated ^{3}H–DNP-GS uptake was not affected appreciably by *Bn*-NCC-1. The K_m and V_{max} values for AtMRP2-dependent ^{3}H–DNP-GS uptake in the presence of 15 μM *Bn*-NCC-1 (80.5 ± 28.6 μM and 18.3 ± 1.6 nmol/mg per 10 min) (Figure 8) were similar to those measured in its absence (Table 1).

AtMRP1, by contrast, transported *Bn*-NCC-1 at such low affinity that saturation by this substrate was not detectable over the concentration range examined (Figure 6A and Table 1).

Table 1. Kinetic Parameters for Uncoupler-Insensitive AtMRP1- and AtMRP2-Dependent Transport of GS Derivatives *Bn*-NCC-1 and Taurocholate[a]

	AtMRP1[b]		AtMRP2[b]	
Compound	K_m	V_{max}	K_m	V_{max}
DNP-GS	73.8 ± 18.8	8.2 ± 1.6	65.7 ± 29.8	16.3 ± 3.1
GSSG	219.2 ± 58.3	6.8 ± 1.1	73.0 ± 15.1	38.1 ± 3.2
Metolachlor-GS	63.6 ± 36.5	17.5 ± 5.2	75.1 ± 31.6	136.0 ± 28.1
Bn-NCC-1	Linear[c]	Linear	15.2 ± 2.3	63.1 ± 2.5
Taurocholate	Linear	Linear	Linear	Linear

[a] Mg-ATP–dependent, uncoupler-insensitive uptake by DTY168/pYES3-AtMRP1, DTY168/pYES3-AtMRP2, and DTY168/pYES3 membranes was measured as described in the legend to Figure 6.
[b] The K_m (μM) and V_{max} (nmol/mg/10 min) values were estimated by fitting the data to a single Michaelis–Menten function by nonlinear least squares analysis (Marquardt, 1963). Values shown are means ±SE.
[c] Uptake increased as a linear function of substrate concentration.

Although neither AtMRP2 nor AtMRP1 transported taurocholate (Figure 6), AtMRP2-mediated transport was selectively inhibited by this compound. AtMRP1-dependent ^{3}H–DNP-GS uptake was relatively insensitive to taurocholate (I_{50} > 250 μM; Figure 9A), but the uptake of both ^{3}H–DNP-GS and ^{14}C–*Bn*-NCC-1 by AtMRP2 was strongly inhibited ($I_{50\ (\text{DNP-GS uptake})}$ = 27 ± 1.3 μM; $I_{50(Bn\text{-NCC-1 uptake})}$ = 49.5 ± 0.3 μM) (Figures 9A and 9B).

Taurocholate at the concentrations used appeared to exert its effect on AtMRP2-mediated transport by inhibiting pump activity directly rather than by increasing background membrane permeability and decreasing net influx by increasing passive DNP-GS efflux. Addition of taurocholate at a concentration (50 μM) sufficient to inhibit AtMRP2-dependent ^{3}H–DNP-GS uptake by 70% (Figure 9A) to DTY168/pYES3-AtMRP2 vesicles that had accumulated ^{3}H–DNP-GS for 10 min before arresting pump action by ATP depletion, using a hexokinase trap, did not accelerate the efflux of intravesicular ^{3}H label over that measured on vesicles subject to a hexokinase trap in the absence of taurocholate (Figure 9C). Imposition of a hexokinase trap and addition of a concentration of detergent (Triton X-100; 0.01% [v/v]) known to permeate these membranes (Zhen et al., 1997), on the other hand, increased the rate and extent of release of the ^{3}H–DNP-GS accumulated during the preceding 10-min uptake period by more than threefold versus DTY168/pYES3-AtMRP2 vesicles treated with hexokinase alone or hexokinase plus taurocholate (Figure 9C).

DISCUSSION

Reconstitution of Mg-ATP–energized, vanadate-inhibitable GS conjugate transport in membranes from yeast *ycf1Δ* cells by the expression of plasmid-borne *AtMRP2* indicates that a second Arabidopsis GS conjugate pump has been cloned. Therefore, it is apparent that GS conjugate pump activity is encoded by a multigene family in this organism. Equally apparent, however, is the divergence of function between AtMRP1 and AtMRP2. Not only does AtMRP2 transport GS conjugates with an order of preference distinct from that of AtMRP1, but it has the facility, which AtMRP1 lacks, for high-affinity transport of the nonglutathionated chlorophyll

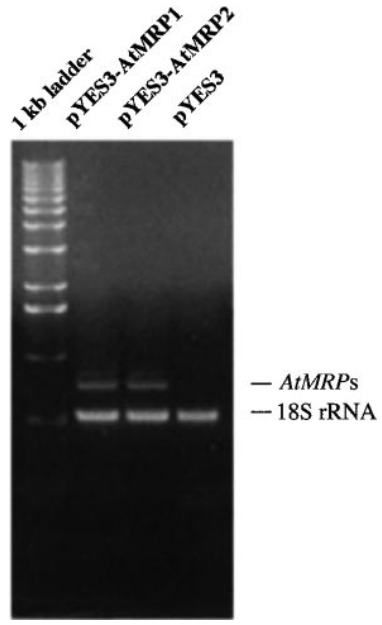

Figure 7. Comparison of Steady State Levels of *AtMRP1* and *AtMRP2* Transcripts in *S. cerevisiae* Strain DTY168 Transformed with pYES3-AtMRP1 or pYES3-AtMRP2, Respectively.

Shown are the products of quantitative RT-PCR of total RNA extracted from these and DTY168/pYES3 cells, using primers delimiting 800 bp of *AtMRP1* and *AtMRP2* and 600 bp of *S. cerevisiae* 18S rRNA.

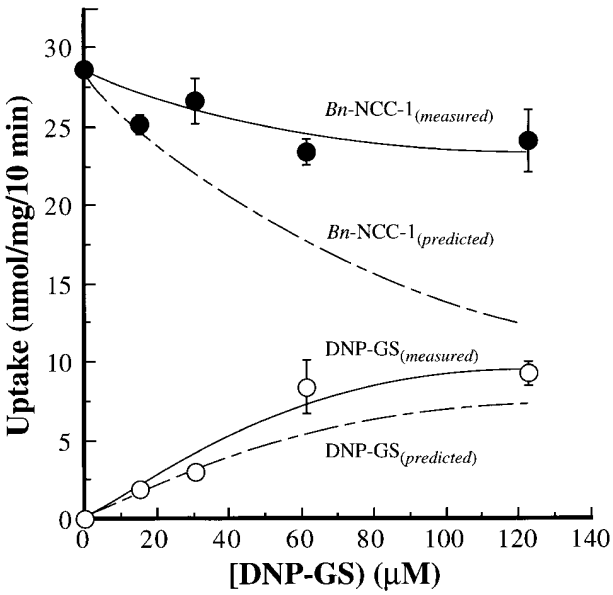

Figure 8. Simultaneous Uptake of *Bn*-NCC-1 and DNP-GS into Vacuolar Membrane–Enriched Vesicles Purified from DTY168/pYES3-AtMRP2 Cells.

Mg-ATP–dependent, uncoupler-insensitive uptake of ^{14}C–*Bn*-NCC-1 and ^{3}H–DNP-GS from media containing a single concentration of ^{14}C–*Bn*-NCC-1 (15 μM) and a range of ^{3}H–DNP-GS concentrations was measured as described in the legend to Figure 6. Solid lines indicate lines of best fit for the experimental data. Dashed lines indicate rates of uptake predicted if *Bn*-NCC-1 were a simple competitive inhibitor of DNP-GS uptake and vice versa. The predicted rates of uptake were calculated from the expression $v = \{V_{max}[S]\}/\{K_m(1 + [I]/K_i) + [S]\}$, where v is the rate of uptake, V_{max} is the maximal rate of uptake, [S] is the concentration of the transport substrate, K_m is the Michaelis constant, [I] is the concentration of inhibitor, and K_i is the inhibition constant for inhibitor I. Simple competitive inhibition of DNP-GS uptake by *Bn*-NCC-1 was estimated by assuming that the K_m for *Bn*-NCC-1 transport (Table 1, 15.2 μM) approximates its K_i for inhibition of DNP-GS uptake. Simple competitive inhibition of *Bn*-NCC-1 uptake by DNP-GS was estimated in the same way, except that the K_m for DNP-GS transport (Table 1, 65.7 μM) was assumed to approximate its K_i for inhibition of *Bn*-NCC-1 uptake. The data for ^{3}H–DNP-GS uptake conformed to a Michaelis–Menten function with a K_m and V_{max} of 80.5 ± 28.6 μM and 18.3 ± 1.6 nmol/mg per 10 min, respectively. Values shown are means ±SE ($n = 3$).

catabolite *Bn*-NCC-1. Indeed, of all the compounds found to be transported by AtMRP2, *Bn*-NCC-1 was transported with the highest affinity.

The exact meaning of the greater transport capacity of heterologously expressed AtMRP2 versus AtMRP1 is not known and depends on the results of investigations of the efficiencies of incorporation of the two polypeptides into the vacuolar membrane–enriched fraction from yeast cells (Z.-S. Li and P.A. Rea, unpublished data); however, the RT-PCR studies described here indicate that the two cDNAs are transcribed at similar rates. Therefore, we tentatively conclude, pending the results of direct immunological assays for the corresponding polypeptides, that AtMRP2 and AtMRP1 are incorporated into the active membrane fraction with similar efficiencies and that the greater transport activity of AtMRP2 is a property intrinsic to this pump.

It was surprising to find that AtMRP2 can transport both *Bn*-NCC-1 and GS conjugates at high affinity because the functionality, and by implication the pump, responsible for Mg-ATP–energized *Bn*-NCC-1 uptake by barley vacuoles had earlier been concluded to be different from that responsible for GS conjugate uptake (Hinder et al., 1996). It is now clear, however, that a reconciliation of the seeming conflict between the findings reported by Hinder et al. (1996) and those reported here is provided by the unusual kinetics of AtMRP2. The capacity of AtMRP2 for the simultaneous transport of *Bn*-NCC-1 and GS conjugates without either substrate interfering with the transport of the other shows that semiautonomous transport of *Bn*-NCC-1 and GS conjugates does not preclude coresidence of both functionalities on the same pump.

Two corollaries—one methodological and the other mechanistic—follow from this characteristic of AtMRP2, and possibly its equivalents from other organisms. (1) The lack of competition between a candidate transport substrate and an established substrate does not automatically imply that the former is not itself transported. It is crucial to test directly for transport rather than rely on competition with an established substrate for the identification of a new transport substrate for this group of transporters. If the equivalent pumps of plants other than Arabidopsis are, like AtMRP2, able to transport *Bn*-NCC-1 and GS conjugates simultaneously (Figure 10), then each of these would be misidentified as two pumps if the sole criterion for nonidentity were lack of competition between transport substrates. (2) Two functionally distinguishable domains appear to reside on AtMRP2. One domain transports GS conjugates, and the other transports compounds such as *Bn*-NCC-1. Transport through one domain is largely independent of transport through the other. In view of the modular construction of ABC transporters (Hyde et al., 1990) and the fact that AtMRP2 and other members of the MRP subclass contain two homologous halves, each half containing an NBF domain located on the cytosolic face of the membrane and a transmembrane (TM) domain containing multiple transmembrane spans, there is a strong possibility that one NBF-TM pair can transport one class of compounds (e.g., GS conjugates) across the membrane, whereas the other NBF-TM pair transports another class of compounds (e.g., chlorophyll catabolites) (Figure 10).

A situation contrary to that encountered with GS conjugates and *Bn*-NCC-1 applies to taurocholate. Neither AtMRP2 nor AtMRP1 transport taurocholate, but AtMRP2-mediated transport of *Bn*-NCC-1 and GS conjugates is strongly inhibited by this compound. The inhibitory action of taurocholate on AtMRP2-mediated transport is not, how-

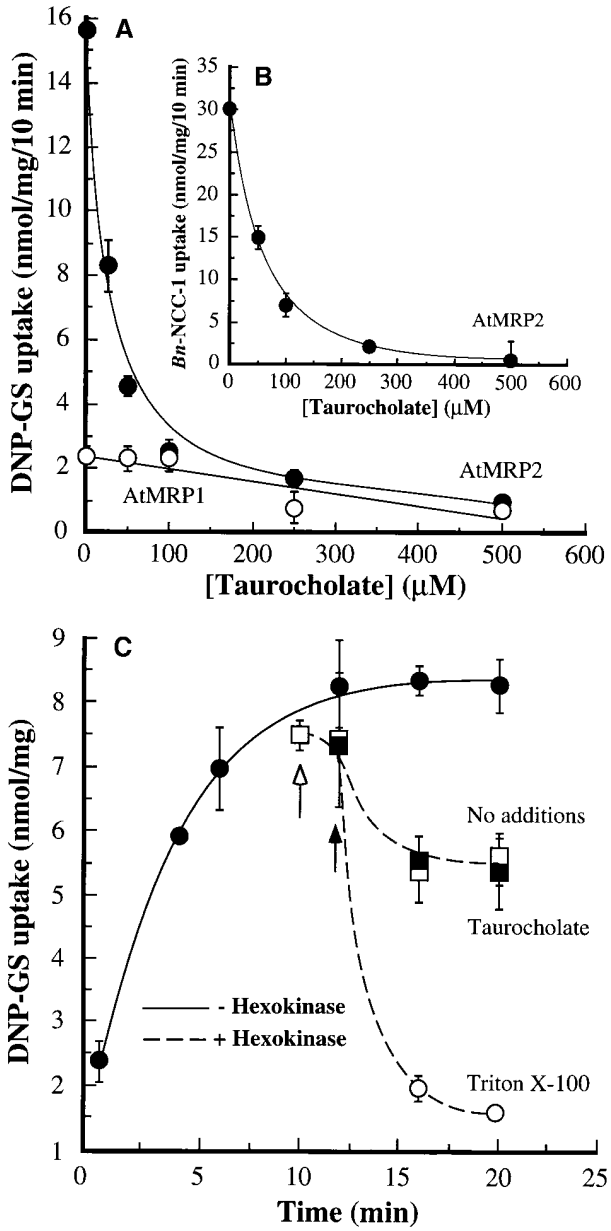

Figure 9. Effects of Taurocholate on AtMRP2- and AtMRP1-Mediated Transport.

(A) Effect of increasing concentrations of taurocholate on AtMRP2- and AtMRP1-dependent uptake of ^{3}H–DNP-GS.

(B) Effect of increasing concentrations of taurocholate on AtMRP2-dependent uptake of ^{14}C–*Bn*-NCC-1. Mg-ATP–dependent, uncoupler-insensitive uptake of ^{14}C–*Bn*-NCC-1 (15 μM) or ^{3}H–DNP-GS (61.3 μM) was measured in media containing the concentrations of unlabeled taurocholate indicated. The rates of AtMRP2- and AtMRP1-dependent uptake were calculated as described in the legend to Figure 6. The I_{50} values for the inhibition of AtMRP2-dependent ^{14}C–*Bn*-NCC-1 and ^{3}H–DNP-GS uptake were estimated to be 49.5 ± 0.3 and 27.7 ± 1.3 μM, respectively, by nonlinear least squares analysis (Marquardt, 1963).

(C) Effect of addition of taurocholate on release of accumulated ^{3}H–DNP-GS from DTY168/pYES3-AtMRP2 membrane vesicles. Mg-ATP–dependent uptake of ^{3}H–DNP-GS was allowed to proceed for 10 min, after which time hexokinase and glucose (+ Hexokinase) were added to the uptake medium (open arrow) to deplete ATP. After another 2 min, taurocholate (50 μM; closed squares) or Triton X-100 (0.01% [v/v]; open circles) was added (closed arrow). No additions were made to the control membranes (− Hexokinase; closed circles).

Values shown are means ±SE (n = 3 or 4).

ever, a detergent effect. The I_{50} values for inhibition of AtMRP2 by taurocholate are 60- to 360-fold lower than is the critical micelle concentration for the detergent, or membrane-permeabilizing action, of this compound (3 to 10 mM). Taurocholate concentrations sufficient to inhibit appreciably AtMRP2-mediated net uptake have no discernible effect on the passive permeability of DTY168/pYES3-AtMRP2 membranes to GS conjugates. AtMRP2-mediated transport is >10 times more sensitive than is AtMRP1-mediated transport to inhibition by taurocholate, which would not be expected if taurocholate exerted its effects by interaction with bulk-phase membrane lipids.

The high sensitivity of both DNP-GS and *Bn*-NCC-1 transport by AtMRP2 and comparative insensitivity of AtMRP1-mediated transport to inhibition by taurocholate indicate that, although this bile salt is relatively specific for AtMRP2 versus AtMRP1, it is capable of inhibiting both of AtMRP2's transport functions. If the idea that one NBF-TM pair of AtMRP2 transports GS conjugates whereas the other transports chlorophyll catabolites is valid, then taurocholate is apparently capable of interacting unproductively with both of these or of binding some other component of AtMRP2 whose interaction with this compound blocks transport through both NBF-TM pairs (Figure 10).

AtMRP2's ability to transport *Bn*-NCC-1 at high efficiency highlights the potential importance of this subclass of plant ABC transporters for the transport of large amphipathic anions other than GS conjugates. Furthermore, the high capacity of AtMRP2 for the transport of both *Bn*-NCC-1 and GS conjugates shows that one pump can assume more than one of the several ABC transporter–like functions identified in plants to date: in the case of AtMRP2, those of both a broad-range GS conjugate pump and chlorophyll catabolite pump. Thus, on the one hand, the high capacity of heterologously expressed AtMRP2, and to a lesser extent AtMRP1, for the transport of metolachlor-GS, and by extension GS conjugates of other herbicides subject to glutathionation in vivo (Kreuz, 1993), is consistent with the molecular identification of transporters capable of removing these and related compounds from the cytosol. On the other hand, the high capacity of AtMRP2 for the transport of *Bn*-NCC-1 is consistent with the identification of an element capable of contributing to the further metabolism and eventual removal of

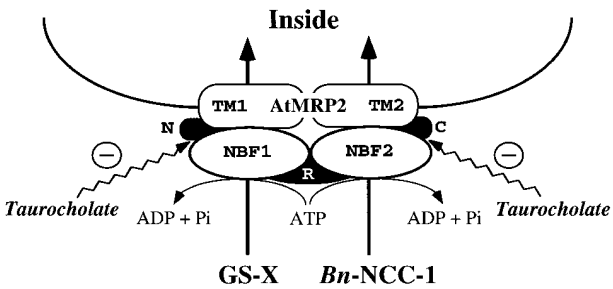

Figure 10. Schematic Diagram Depicting Parallel Transport of GS Conjugates (GS-X) and *Bn*-NCC-1 by AtMRP2.

It is proposed that GS conjugates are transported by one NBF-TM pair (e.g., NBF1-TM1), whereas *Bn*-NCC-1 is transported by the other NBF-TM pair (e.g., NBF2-TM2). It is speculated that taurocholate inhibits transport through both NBF-TM pairs without itself undergoing transport.

tetrapyrrole derivatives generated during leaf senescence from the cytosol.

Conversion of mesophyll chloroplasts into gerontoplasts during leaf senescence and yellowing is accompanied by the disassembly of thylakoid pigment–protein complexes and breakdown of chlorophyll into phytol and water-soluble porphyrin derivatives (Matile, 1992). The water-soluble porphyrins generated are exported from the gerontoplasts and accumulated ultimately in the vacuoles of the senescing cells, where they remain until the end of the senescence period. Three of the principal vacuolar tetrapyrroles of rape (*Bn*-NCC-1, *Bn*-NCC-2, and *Bn*-NCC-3) have been purified and structurally characterized. One, *Bn*-NCC-1, has been shown to undergo Mg-ATP–energized, vanadate-inhibitable uptake into barley vacuoles (Hinder et al., 1996). Hence, although the status of AtMRP2 as a strict ortholog of the endogenous transporter of barley remains to be defined, because the characteristics of heterologously expressed AtMRP2 (K_m = 15 μM; taurocholate sensitivity) deviate from those of barley vacuoles (K_m = 110 μM; taurocholate insensitivity), the molecular investigations reported here nonetheless extend and complement the results of physiological studies to show that a plant MRP subclass ABC transporter has the requisite biochemical capabilities for participation in the vacuolar sequestration of nonglutathionated chlorophyll catabolites during leaf senescence.

Of the two transporters described in this communication, the properties of AtMRP1 better approximate those of the endogenous vacuolar GS conjugate pump of etiolated hypocotyls of mung bean (Li et al., 1995a), one of the most rigorously characterized plant GS conjugate pumps. Steady state levels of *AtMRP1* transcript are constitutively high in stems, and the rates of uptake of 50 μM concentrations of DNP-GS, GSSG, metolachlor-GS, and C3G-GS by heterologously expressed AtMRP1 fall in the same rank order as for mung bean vacuolar membrane vesicles (C3G-GS > metolachlor-GS > DNP-GS ⩾ GSSG; uptake ratio for AtMRP1 = 2.7:1.5:1.0:0.7; uptake ratio for mung bean = 5.5:3.9:1.0:0.8). The properties of AtMRP2, by comparison, suggest a different operational context. The steady state levels of *AtMRP2* transcript are consistently low at the whole-tissue level, and the rates of AtMRP2-dependent GS conjugate transport fall in a rank order (metolachlor-GS > C3G-GS >> GSSG > DNP-GS; uptake ratio = 7.8:6.4:2.2:1.0) distinct from that of AtMRP1 and the endogenous mung bean pump.

Experiments with wild-type and T-DNA insertional *AtMRP1* and *AtMRP2* mutant plants (Y.-P. Lu and P.A. Rea, unpublished data) are in progress to determine whether the constitutively low levels of expression of *AtMRP2* at the tissue level signify its amenability to modulation by exogenous and/or endogenous factors that have yet to be identified and/or a cell distribution that is more restricted than that of AtMRP1. It is known that the steady state levels of RNAs containing sequences overlapping with *AtMRP1* are relatively invariant, whereas those containing sequences overlapping with *AtMRP2* are induced by the cytotoxic DNP-GS precursor 1-chloro-2,4-dinitrobenzene (Tommasini et al., 1997). However, the phenotypic consequences for the intact plant with null mutations in these genes, the effects of exogenous stress factors in addition to xenobiotics, and the expression patterns of individual cell types must be examined before firm conclusions can be drawn for transporters with such a broad functional repertoire.

In view of the functional divergence between AtMRP1 and AtMRP2, the capacity of the endogenous vacuolar GS conjugate pump for high-affinity transport of glutathionated medicarpin, which is an isoflavonoid phytoalexin (Li et al., 1997a), the amenability of C3G-GS, which is an anthocyanin derivative, and GSSG, which is a product of peroxide detoxification and protein thiol reduction, to transport by AtMRP2 and AtMRP1, the processes that will affect *AtMRP* expression, and the phenotypes of null mutants are likely to extend beyond herbicide detoxification and chlorophyll catabolism to include the storage of antimicrobial compounds, cell pigmentation, and the alleviation of oxidative damage.

METHODS

Isolation of *AtMRP2*

AtMRP2 was isolated by a procedure similar to that used for *AtMRP1* (Lu et al., 1997), using degenerate oligonucleotide primers corresponding to the second ATP binding cassette of ScYCF1 and HmMRP1 for the polymerase chain reaction (PCR) amplification of *Arabidopsis thaliana* genomic DNA. The two primers, MRP2 and MRP4 (Table 2), yielding a 0.6-kb PCR product that strongly hybridized with DNA probes encompassing the coding regions of the second ATP binding cassettes of HmMRP1 and ScYCF1, had sequences corresponding to amino acid residues 1300 to 1310 and 1321 to 1331 of ScYCF1 and residues 1466 to 1474 and 1486 to

Table 2. Sequences of the Oligonucleotide Primers Used for the PCR Amplification Reactions Described in This Study

Primer	Sequence[a]
MRP2	5′-GARAARGTIGGIATHGTIGGIMGI-ACIGGIGC-3′
MRP4	5′-TCCATDATIGTRTTIARICKTGIGC-3′
AtMRP-raceB	5′-ACGGCCCTAGCCATGGAAACC-CTCTGCTTC-3′
AtMRP-raceA	5′-TAACGGGTCATCAAAGATGTACAC-ATCTGA-3′
AtMRP2-5S	5′-GCACTGTGTTTGAGGGAAAGGAAA-GGATAACGA-3′
AtMRP2-NcoI	5′-GGATAACCATGGGGTTTGAGTTTA-TTG-3′
AtMTP3S	5′-GACTGGGACAAYGTCGAGATG-3′
pUC/M13-reverse	5′-TCACACAGGAAACAGCTATGAC-3′
AT18S-5	5′-TTGATTCTATGGGTGGTGGT-3′
At18S-3	5′-ACCTATCGACAATGATCCTT-3′
Y18S-5	5′-AGATTAAGCCATGCATGTCT-3′
Y18S-3	5′-TGCTGGTACCAGACTTGCCCTCC-3′
AtMRP1250S	5′-ACATGATTGCTGCTGTGTTC-3′
AtMRP600S	5′-GTCATTTATGCTCTTGTGGG-3′
AtMRP9A1	5′-TCAGTGCTATAATTATACG-3′

[a] D is an A, T, or G residue; K, a T or G residue; M, a C or A residue; and R, an A or G residue.

1494 of HmMRP1 (Cole et al., 1992; Szczypka et al., 1994). After establishing that the 0.6-kb PCR product had greatest similarity to ScYCF1 and HmMRP1 plus the putative translation product of an unidentified 1.6-kb Arabidopsis expressed sequence tag (EST) (ATTS1246) (Hofte et al., 1993), a mixed probe consisting of this and the PCR product was used to screen $\sim 3 \times 10^5$ plaques of a size-fractionated (3- to 6-kb) Arabidopsis cDNA library constructed in λZAPII (Stratagene, La Jolla, CA; Kieber et al., 1993). The cDNA insert of the largest of the clones isolated from this screen was subcloned into pBluescript SK− (Stratagene), sequenced, and found to best align with ScYCF1 and HmMRP1 of all of the sequences in the GenBank/EMBL database release 90 (Altschul et al., 1990).

On the assumption that the complete open reading frame of the gene corresponding to this cDNA was similar in size to those of *ScYCF1* and *HmMRP1*, it was estimated to be missing a minimum of 1.5 kb of 5′ coding sequence. Hence, to isolate clones containing this missing sequence, 500 bp of the 5′ terminal portion of the 3.5-kb cDNA was used to screen two Arabidopsis bacterial artificial chromosome (BAC) libraries, namely, UCD (Wang et al., 1996) and TAMU (Choi et al., 1995). This procedure yielded eight genomic clones: U1L22, U8C12, U12A2, U23J22, U4I9, T9C22, T1B17, and T4K22. DNA gel blot analyses of the BAC clones after digestion with HindIII and hybridization with the same cDNA probe or with a cDNA probe for *AtMRP1* disclosed two major classes: T1B17 and T4K22, which were determined to be genomic clones of the *AtMRP1* gene (Lu et al., 1997), and U1L22, U8C12, U12A2, U23J22, U4I9, and T9C22, which were determined to contain exons with identity to the new 3.5-kb cDNA. The 3.5-kb cDNA was designated *AtMRP2.*

The complete genomic sequence of *AtMRP2* was determined after subcloning the 9-kb HindIII fragment of U1L22 and 6-kb BglII fragment of U12A2 into pBluescript SK−. The 5′ coding sequence missing from the cDNA was obtained by reverse transcriptase (RT)–PCR. Total RNA (5 μg) from 5-week-old plants was used to generate the first-strand cDNA with Superscript II RNase H^- RT (Bethesda Research Laboratories), using primer AtMRP-raceA (Table 2). Amplification was performed by PCR, using the nested primers AtMRP-raceB and AtMRP2-5S (Table 2), the latter of which corresponded to the sequence of a portion of the 5′ untranslated region of *AtMRP2* identified in the genomic sequence. The 2.3-kb product from this reaction was cloned into pCRII (Invitrogen) to generate pCR-AtMRP2. After confirming that it encompassed the missing 5′ portion of *AtMRP2* by sequencing, the 2.3-kb fragment of XhoI-NcoI–digested pCR-AtMRP2 was inserted into the SalI-NcoI sites of the 3.5-kb subclone in pBluescript SK− to yield plasmid (pAtMRP2) containing the full-length cDNA.

Determination of Physical Map Position of *AtMRP2*

Primers AtMRP1250S and AtMRP19A1 (Table 2) were used for PCR amplification of 24 DNA pools from yeast artificial chromosome (YAC) library YUP (Ecker, 1991) and 12 DNA pools from YAC library CIC (Creusot et al., 1995), of which four pools (YIP16, CIC9, CIC10, and CIC12) yielded a 0.5-kb product with the sequence of *AtMRP2.* To identify the individual YAC clones containing *AtMRP2*, the same primers were used to screen each of the 20 YAC clones in each of the positive DNA pools, thus identifying YUP16C2, CIC9H2, CIC10F1, and CIC12G9 as encompassing *AtMRP2.* A search of the Arabidopsis BAC end sequence database (http://www.tigr.org/tdb/at/atgenome/bac_end_search/bac_end_search.html) disclosed that the 11-kb genomic sequence of *AtMRP2* corresponded to BAC clones T9C22, T25H7, T29F13, T31E10, F15G8, and T28P19. Hybridization between these BAC clones and the positive YAC clones from the PCR screens confirmed that CIC9H2 and CIC12G9 encompassed T9C22, T25H7, T29F13, and T31E10, whereas CIC10F1 encompassed T29F13. Because all three CIC YAC clones mapped to a position between Ve016 and Ve018 on chromosome 2 (S. Rounsley and H. Goodman, personal communication), *AtMRP2* was assigned to this position.

RNA Gel Blot Analyses

The steady state levels of *AtMRP2* and *AtMRP1* transcripts in different tissues from Arabidopsis plants were determined by RNA gel blot analysis. Total RNA was extracted from roots, stems, leaves, and flowers of 5-week-old plants, as described previously (Lu et al., 1997). The RNA samples were resolved on 10% (v/v) formaldehyde–agarose gels, transferred to Hybond-N^+ membrane filters (Amersham Corp., Arlington Heights, IL), and baked at 80°C for 2 hr. The filters were prehybridized in 7% (w/v) SDS, 1 mM EDTA, and 0.3 M sodium phosphate buffer, pH 7.2, at 65°C for 3 hr before hybridization overnight in the same buffer containing ^{32}P-labeled *AtMRP2*- or *AtMRP1*-specific riboprobe. The filters were washed twice in 1 × standard saline citrate and 0.1% (w/v) SDS (5 min at room temperature) and once in 0.2 × standard saline citrate and 0.1% (w/v) SDS (15 min at 65°C). ^{32}P-labeled bands were visualized and quantitated using a PhosphorImager (Molecular Dynamics, Sunnyvale, CA).

AtMRP2- and *AtMRP1*-specific riboprobes were transcribed from 184- and 224-bp PCR amplification products corresponding to the 3′ untranslated regions of pAtMRP2 and pAtMRP1 (Lu et al., 1997), respectively, generated using primers AtMRP3S and pUC/M13-reverse

(Table 2). After purification of the PCR products on QIAquick spin-columns (Qiagen Inc., Valencia, CA), ^{32}P-labeled antisense RNAs were synthesized from the DNA templates by using T3 RNA polymerase (Stratagene). The riboprobes were separated by PAGE, eluted by overnight incubation in 0.5 M ammonium acetate, 1 mM EDTA, and 0.2% (w/v) SDS, and added to the hybridization buffer at a final radioactivity of 5×10^6 cpm/mL.

To ensure equal loading of the RNA samples, 18S rRNA was used as an internal standard. Primers At18S-5 and At18S-3 (Table 2) were used to amplify a 500-bp fragment of EST clone 40F8T7 corresponding to the 18S rRNA gene from Arabidopsis (GenBank accession number T04433) (Newman et al., 1994). ^{32}P-labeled DNA probe was prepared using a random priming kit (Promega). The *AtMRP1*, *AtMRP2*, and rRNA probes were applied individually to the same blots after stripping the filters twice in boiling 0.1% (w/v) SDS between analyses.

Isolation of *Bn*-NCC-1

^{14}C–*Bn*-NCC-1 (33.3 mCi/mmol) was extracted from senescent cotyledons of oilseed rape (*Brassica napus*) and purified by preparative HPLC. Determination of the purity of the final preparation and enumeration of concentration and specific radioactivity (33.3 mCi/mmol) were according to Hinder et al. (1996). Unlabeled *Bn*-NCC-1 was isolated from fully senescent cotyledons of excised shoots that had been kept in complete darkness for 1 week.

Preparation and Purification of Glutathionated Compounds

^{3}H–DNP-GS (17.4 mCi/mmol) was synthesized enzymically from 1-chloro-2,4-dinitrobenzene and ^{3}H-GSH (Li et al., 1995a). ^{3}H-GSSG was synthesized enzymically by incubation of 100 μM ^{3}H-GSH (44 Ci/mmol) and 100 μM hydrogen peroxide with 10 units of glutathione peroxidase (type III from baker's yeast) for 4 hr at 25°C in 10 mM phosphate buffer, pH 7.5 (Lu et al., 1997). ^{14}C–metolachlor-GS and ^{3}H–DNP-GS were synthesized by general base catalysis. ^{14}C–metolachlor-GS was synthesized by adding 100 μM GSH and 50 μM ^{14}C-metolachlor (8.3 mCi/mmol) to 25 mM sodium borate buffer, pH 9.0, and incubating overnight at 55°C (Li et al., 1995a; Lu et al., 1997). ^{3}H–C3G-GS was synthesized by adding 100 μM ^{3}H-GSH (17.4 mCi/mmol) and 50 μM C3G to the same buffer system. All of the conjugates were purified by reverse-phase fast protein liquid chromatography, as described previously (Li et al., 1995a).

Heterologous Expression of *AtMRP2* in *Saccharomyces cerevisiae ycf1Δ* Mutants

For constitutive expression in *S. cerevisiae*, *AtMRP2* cDNA from which the 5′ untranslated region had been removed by PCR, using primer AtMRP2-NcoI (Table 2), was inserted into the multiple cloning site between the 3-phosphoglycerate kinase (*PGK*) gene promoter and cytochrome c_1 gene (*CYC1*) termination sequences of the yeast–*Escherichia coli* shuttle vector pYES3 (Lu et al., 1997). After confirming the fidelity of the construct by sequencing, *S. cerevisiae ycf1Δ* strain DTY168 (*MATα his6 leu2-3,-112 ura3-52 ycf1*::*hisG*) (Szczypka et al., 1994) was transformed with pYES3-AtMRP2 or an empty vector lacking the *AtMRP2* insert (pYES3) by the LiOAc/polyethylene glycol method (Gietz and Schiestl, 1991) and selected for uracil prototrophy by plating on AHC medium containing tryptophan (Kim et al., 1995). Heterologous expression of *AtMRP1* was accomplished using a similar procedure (Lu et al., 1997).

Quantitative RT-PCR

The levels of *AtMRP2* and *AtMRP1* transcripts in pYES3-AtMRP2– and pYES3-AtMRP1–transformed yeast DTY168 cells, respectively, were estimated by RT-PCR. Total RNA was extracted from DTY168/pYES3-AtMRP2, DTY168/pYES3-AtMRP1, and DTY168/pYES3 cells, as described previously (Sherman et al., 1983), and 1-μg samples were reverse transcribed using Superscript II RNase H$^-$ RT (Bethesda Research Laboratories). Each of the first-strand cDNA products was amplified by PCR, using primers AtMRP600 and AtMRP9A1 (Table 2), whose sequences are identical in both *AtMRP1* and *AtMRP2.* To determine whether the same amounts of RNA had been sampled from the three transformants, two primers, Y18S-5 and Y18S-3 (Table 2), corresponding to the sequence of *S. cerevisiae* 18S rRNA, were also added to the reactions. PCR amplification was performed using the following thermal profile: 3 min at 96°C, 20 cycles of 20 sec at 97°C, 20 sec at 55°C, and 1 min at 72°C. The PCR products were separated on 1% agarose gels and stained with ethidium bromide. Controls were subjected to PCR without reverse transcription to test for contamination of the RNA samples with genomic DNA.

Measurement of Transport

Cells were grown and vacuolar membrane–enriched vesicles were prepared as described by Kim et al. (1995). Uptake of ^{14}C–*Bn*-NCC-1, ^{3}H–C3G-GS, ^{3}H–DNP-GS, ^{3}H-GSSG, ^{14}C-metolachlor, or ^{3}H-taurocholate was measured routinely in 200-μL reaction volumes containing membrane vesicles (10 to 20 μg of protein), 3 mM ATP, 3 mM $MgSO_4$, 5 μM gramicidin D, 10 mM creatine phosphate, 16 units/mL creatine phosphate kinase, 50 mM KCl, 1 mg/mL BSA, 400 mM sorbitol, 25 mM Tris–Mes, pH 8.0, and the indicated concentrations of transport substrate. Uptake was terminated by the addition of 1 mL of ice-cold wash medium (400 mM sorbitol and 3 mM Tris–Mes, pH 8.0) and vacuum filtration of the suspension through prewetted Millipore HA cellulose nitrate filters (pore size, 0.45 μm). The filters were rinsed twice with wash medium, and the radioactivity retained was determined by liquid scintillation counting. Nonenergized uptake was estimated by the same procedure except that ATP was omitted from the uptake medium.

The effect of taurocholate on the release of ^{3}H–DNP-GS from membrane vesicles that had been allowed to mediate AtMRP2-dependent accumulation of this compound during a preceding uptake period was determined by rapid depletion of ATP from the uptake medium by using a hexokinase trap (glucose + ATP $\rightarrow$ glucose 6-phosphate + ADP) and measurements of the decrease in vesicular radiolabel in the presence or absence of taurocholate. Membranes from DTY168/pYES3-AtMRP2 cells were incubated for 10 min in standard uptake medium containing 61.3 μM ^{3}H–DNP-GS, after which time 200 mM glucose and 50 units per mL hexokinase (type F-300 from baker's yeast) were added. After incubation for an additional 2 min, taurocholate (50 μM) or Triton X-100 (0.01% [v/v]) was added, and release of vesicular ^{3}H–DNP-GS was measured as de-

scribed above. Control samples were treated identically, except that no additions were made after the initial 10-min incubation period.

Measurement of Protein

Protein was estimated by a modification of the Lowry method (Peterson 1977).

Chemicals

Glutathione peroxidase and hexokinase, ^{3}H-GSH and ^{3}H-taurocholate, and cyanidin-3-glucoside were purchased from Sigma, Du Pont–New England Nuclear Research, and EXTRASYNTHESE S.A. (Genay, France), respectively. ^{14}C-metolachlor was a gift from CIBA-Geigy (Greensboro, NC). All of the general reagents, which were of the highest quality, were obtained from Fisher Scientific (Pittsburgh, PA), Research Organics Inc. (Cleveland, OH), or Sigma.

Accession Numbers

The cDNA and genomic sequences reported here have GenBank accession numbers AF020288 and AF020289, respectively, for *AtMRP2* and AF008124 and AF008125, respectively, for *AtMRP1.*

ACKNOWLEDGMENTS

We thank Drs. Steven Rounsley (Institute for Genomic Research, Rockville, MD) and Howard M. Goodman (Massachusetts General Hospital, Boston, MA) for providing unpublished Arabidopsis chromosome mapping data; Joe Ecker and colleagues for the YAC and BAC library filters used in these investigations; Junsheng Zhan and Melinda Moy for technical assistance; and Rui-Guang Zhen and Ji-Dong Feng for technical advice. This work was funded by grants from the U.S. Department of Agriculture (National Research Initiative Competitive Grants Program No. 93-37304-8932) and U.S. Department of Energy (No. DE-FG02-91ER20055) awarded to P.A.R. Y.M.D. is a Triagency (U.S. Department of Energy/National Science Foundation/U.S. Department of Agriculture) Plant Training Grant Fellow.

Received October 10, 1997; accepted December 3, 1997.

REFERENCES

Altschul, S.F., Gish, W., Miller, W., Myers, E.W., and Lipman, D. (1990). Basic local alignment search tool. J. Mol. Biol. **215,** 403–410.

Blake-Kalff, M.M.A., and Coleman, J.O.D. (1996). Detoxification of xenobiotics by plant cells: Characterisation of vacuolar amphiphilic organic anion transporters. Planta **200,** 426–431.

Choi, S., Creelman, R.A., and Wing, R.A. (1995). Construction and characterization of a bacterial artificial chromosome library from *Arabidopsis thaliana*. Weeds World **2,** 17–20.

Cole, S.P.C., Bhardwaj, G., Gerlach, J.H., Mackie, J.E., Grant, C.E., Almquist, K.C., Stewart, A.J., Kurz, E.U., Duncan, A.M.V., and Deeley, R.G. (1992). Overexpression of a transporter gene in a multidrug-resistant human lung cancer cell line. Science **258,** 1650–1654.

Creusot, F., Fouilloux, E., Dron, M., Lafleuriel, J., Pickard, G., Billault, A., Lepaslier, D., Cohen, D., Chaboute, M.E., Durr, A., Fleck, J., Gigot, C., Camilleri, C., Bellini, C., Caboche, M., and Bouchez, D. (1995). The CIC library: A large insert YAC library for genome mapping in *Arabidopsis thaliana.* Plant J. **8,** 763–770.

Davies, T.G.E., Theodoulou, F.L., Hallahan, D.L., and Forde, B.G. (1997). Cloning and characterization of a novel P-glycoprotein homologue from barley. Gene **199,** 195–202.

Dudler, R., and Hertig, C. (1992). Structure of an *mdr*-like gene from *Arabidopsis thaliana*: Evolutionary implications. J. Biol. Chem. **267,** 5882–5888.

Ecker, J.R. (1991). PFGE and YAC analysis of the *Arabidopsis* genome. Methods **1,** 186–194.

Gietz, R.D., and Schiestl, R.H. (1991). Applications of high efficiency lithium acetate transformation of intact yeast cells using single-stranded nucleic acids as carrier. Yeast **7,** 253–263.

Higgins, C.F. (1992). ABC transporters: From microorganisms to man. Annu. Rev. Cell Biol. **8,** 67–113.

Hinder, B., Schellenberg, M., Rodon, S., Ginsburg, S., Vogt, E., Martinoia, E., Matile, P., and Hortensteiner, S. (1996). How plants dispose of chlorophyll catabolites. Directly energized uptake of tetrapyrrolic breakdown products into isolated vacuoles. J. Biol. Chem. **271,** 27233–27236.

Hofte, H., Desprez, T., Amselem, J., Chiapello, H., Caboche, M., Moisan, A., Jourjon, M.F., Charpenteau, J.L., Berthomieu, P., Guerrier, D., Giraudat, J., Quigley, F., Thomas, F., Yu, D.Y., Mache, R., Raynal, M., Cooke, R., Grellet, F., Delseny, M., Parmentier, Y., Demarcillac, G., Gigot, C., Fleck, J., Philipps, G., Axelos, M., Bardet, C., Tremousaygue, D., and Lescure, B. (1993). An inventory of 1152 expressed sequence tags obtained by partial sequencing of cDNAs from *Arabidopsis thaliana.* Plant J. **4,** 1051–1061.

Hörtensteiner, S., Vogt, E., Hagenbuch, B., Meier, P.J., Amrheim, N., and Martinoia, E. (1993). Direct energization of bile acid transport into plant vacuoles. J. Biol. Chem. **268,** 18446–18449.

Huber, M., Guhlmann, A., Jansen, P.L.M., and Keppler, D. (1987). Hereditary defect of hepatobiliary cysteinyl leukotriene elimination in mutant rats with defective hepatic anion excretion. Hepatology **7,** 224–228.

Hyde, S.C., Elmsley, P., Hartshom, M.J., Mimmack, M.M., Gileadi, U., Pearce, S.R., Gallagher, M.P., Gill, D.R., Hubbard, R.E., and Higgins, C.F. (1990). Structural model of ATP-binding proteins associated with cystic fibrosis, multidrug resistance and bacterial transport. Nature **346,** 362–365.

Ishikawa, T., Muller, M., Klunemann, C., Shaub, T., and Keppler, D. (1990). ATP-dependent primary active transport of cysteinyl leukotrienes across liver canalicular membrane. Role of the ATP-dependent transport system for glutathione *S*-conjugates. J. Biol. Chem. **265,** 19279–19286.

Ishikawa, T., Li, Z.-S., Lu, Y.-P., and Rea, P.A. (1997). The GS-X pump in plant, yeast, and animal cells: Structure, function, and gene expression. Biosci. Rep. **17,** 189–207.

Jedlitschky, G., Leier, I., Buchhoz, U., Barnouin, K., Kurz, G., and Keppler, D. (1996). Transport of glutathione, glucuronate, and sulfate conjugates by the *MRP* gene–encoded conjugate export pump. Cancer Res. **56,** 988–994.

Kieber, J.J., Rothenberg, M., Roman, G., Feldman, K.A., and Ecker, J.R. (1993). CTR1, a negative regulator of the ethylene response pathway in Arabidopsis, encodes a member of the Raf family of protein kinases. Cell **72,** 427–441.

Kim, E.J., Zhen, R.-G., and Rea, P.A. (1995). Site-directed mutagenesis of vacuolar H^+-pyrophosphatase. Necessity of Cys^{634} for inhibition by maleimides but not catalysis. J. Biol. Chem. **270,** 2630–2635.

Kreuz, K. (1993). Herbicide safeners: Recent advances and biochemical aspects of their mode of action. In Proceedings of Brighton Crop Protection Conference: Weeds (Brighton, UK: Academic Press), pp. 1249–1258.

Kyte, J., and Doolittle, R.F. (1982). A simple method for displaying the hydropathic character of a protein. J. Mol. Biol. **157,** 105–132.

Leier, I., Jedlitschky, G., Buchholz, U., Cole, S.P.C., Deeley, R.G., and Keppler, D. (1994). The *MRP* gene encodes an ATP-dependent export pump for leukotriene C_4 and structurally related conjugates. J. Biol. Chem. **269,** 27807–27810.

Li, Z.-S., Zhao, Y., and Rea, P.A. (1995a). Magnesium adenosine 5′-triphosphate–energized transport of glutathione *S*-conjugates by plant vacuolar membrane vesicles. Plant Physiol. **107,** 1257–1268.

Li, Z.-S., Zhen, R.-G., and Rea, P.A. (1995b). 1-Chloro-2,4-dinitrobenzene–elicited increase in vacuolar glutathione *S*-conjugate transport activity. Plant Physiol. **109,** 177–202.

Li, Z.-S., Szczypka, M., Lu, Y.-P., Thiele, D.J., and Rea, P.A. (1996). The yeast cadmium factor protein (YCF1) is a vacuolar glutathione *S*-conjugate pump. J. Biol. Chem. **271,** 6509–6517.

Li, Z.-S., Alfenito, M.R., Rea, P.A., Walbot, V., and Dixon, R.A. (1997a). Vacuolar uptake of the phytoalexin medicarpin by the glutathione conjugate pump. Phytochemistry **45,** 689–693.

Li, Z.-S., Lu, Y.-P., Zhen, R.-G., Szczypka, M., Thiele, D.J., and Rea, P.A. (1997b). A new pathway for vacuolar cadmium sequestration in *Saccharomyces cerevisiae*: YCF1-catalyzed transport of *bis*(glutathionato)cadmium. Proc. Natl. Acad. Sci. USA **94,** 42–47.

Lu, Y.-P., Li, Z.-S., and Rea, P.A. (1997). *AtMRP1* of *Arabidopsis thaliana* encodes a glutathione *S*-conjugate pump: Isolation and functional definition of a plant ATP-binding cassette transporter gene. Proc. Natl. Acad. Sci. USA **94,** 8243–8348.

Marquardt, D.W. (1963). An algorithm for least squares estimation of nonlinear parameters. J. Soc. Ind. Appl. Math. **11,** 431–441.

Martinoia, E., Grill, E., Tommasini, R., Kreuz, K., and Amrheim, N. (1993). ATP-dependent glutathione *S*-conjugate 'export' pump in the vacuolar membrane of plants. Nature **364,** 247–249.

Matile, P. (1992). In Crop Photosynthesis: Spatial and Temporal Determinants, N.R. Baker and H. Thomas, eds (Amsterdam: Elsevier Science Publishers), pp. 413–440.

Muller, M., Meijer, C., Zaman, G.J.R., Borst, P., Scheper, R.J., Mulder, N.H., de Vries, E.G.E., and Jansen, P.L.M. (1994). Overexpression of the gene encoding the multidrug resistance associated protein results in increased ATP-dependent glutathione *S*-conjugate transport. Proc. Natl. Acad. Sci. USA **91,** 13033–13037.

Newman, T., de Bruijn, F.J., Green, P., Keegstra, K., Kende, H., McIntosh, L., Ohlrogge, J., Raikhel, N., Somerville, S., Thomashow, M., Retzel, E., and Somerville, C. (1994). Genes galore: A summary of methods for accessing results from large-scale partial sequencing of anonymous *Arabidopsis* cDNA clones. Plant Physiol. **106,** 1241–1255.

Paulusma, C.C., Bosma, P.J., Zaman, G.J.R., Bakker, C.T.M., Otter, M., Scheffer, G.L., Scheper, R.J., Borst, P., and Elferink, R.P.J.O. (1996). Congenital jaundice in rats with a mutation in a multidrug resistance–associated protein gene. Science **271,** 1126–1128.

Peterson, G.L. (1977). Review of the Folin phenol protein quantitation method of Lowry, Rosebrough, Farr and Randall. Anal. Biochem. **83,** 346–356.

Sathirakul, K., Susuki, H., Yamada, T., Hanano, M., and Sugiyama, Y. (1993). Kinetic analysis of hepatobiliary transport of organic anions in Eisai hyperbilirubinemic mutant rats. J. Pharmacol. Exp. Ther. **268,** 65–73.

Sherman, F., Fink, G.R., and Hicks, J.R. (1983). Methods in Yeast Genetics. (Plainview, NY: Cold Spring Harbor Laboratory Press).

Szczypka, M.S., Wemmie, J.A., Moye-Rowley, W.S., and Thiele, D.J. (1994). A yeast metal resistance protein similar to human cystic fibrosis transmembrane conductance regulator (CFTR) and multidrug resistance–associated protein. J. Biol. Chem. **269,** 22853–22857.

Tommasini, R., Evers, R., Vogt, E., Mornett, C., Zaman, G.J.R., Schinkel, A.H., Borst, P., and Martinoia, E. (1996). The human multidrug resistance associated protein functionally complements the yeast cadmium resistance factor 1. Proc. Natl. Acad. Sci. USA **93,** 6743–6748.

Tommasini, R., Vogt, E., Schmid, J., Fromentau, M., Amrheim, N., and Martinoia, E. (1997). Differential expression of genes coding for ABC transporters after treatment of *Arabidopsis thaliana* with xenobiotics. FEBS Lett. **411,** 206–210.

Wang, W., Takezawa, D., and Pooviah, B.W. (1996). A potato cDNA encodes a homologue of mammalian multidrug resistance P-glycoprotein. Plant Mol. Biol. **31,** 683–687.

Zhen, R.-G., Kim, E.J., and Rea, P.A. (1997). Acidic residues necessary for pyrophosphate-energized pumping and inhibition of the vacuolar H^+-pyrophosphatase by *N*,*N*′-dicyclohexylcarbodiimide. J. Biol. Chem. **272,** 22340–22348.